Inorganic Chemistry

Article

pubs.acs.org/IC

$KSbB_2O_6$ and $BaSb_2B_4O_{12}$: Novel Boroantimonates with 3D Anionic Architectures Composed of 1D Chains of SbO_6 Octahedra and B_2O_5 Groups

Chao Huang,[†,‡] Jian-Han Zhang,[†] Chun-Li Hu,[†] Xiang Xu,[†] Fang Kong,[†] and Jiang-Gao Mao*[,†]

[†]State Key Laboratory of Structural Chemistry, Fujian Institute of Research on the Structure of Matter, Chinese Academy of Sciences, 155 Yangqiao Road West, Fuzhou 350002, People's Republic of China

[‡]University of Chinese Academy of Sciences, Beijing, 100039, People's Republic of China

Supporting Information

ABSTRACT: Two new boroantimonates, namely, $KSbB_2O_6$ and $BaSb_2B_4O_{12}$, have been successfully synthesized through high-temperature solid state reactions. Their structures feature two types of novel anionic 3D frameworks composed of 1D chains of corner-sharing SbO_6 octahedra that are interconnected by B_2O_5 groups. The 1D chains of corner-sharing SbO_6 octahedra in polar $KSbB_2O_6$ (space group Cc) are extended along the c-axis, whereas those in the centrosymmetric $BaSb_2B_4O_{12}$ (space group $C2/c$) are propagated along the [101] direction. The K^+ ions are located at the 1D tunnels of the anionic frameworks along both b- and c-axis, whereas Ba^{2+} ions are located at the 1D tunnels of the anionic frameworks along both the a- and c-axis. $KSbB_2O_6$ is a polar material that displays weak SHG response, whereas $BaSb_2B_4O_{12}$ is centrosymmetric and not SHG active. Studies on their optical properties, thermal stability, and band structure calculations based on DFT methods have been also performed.

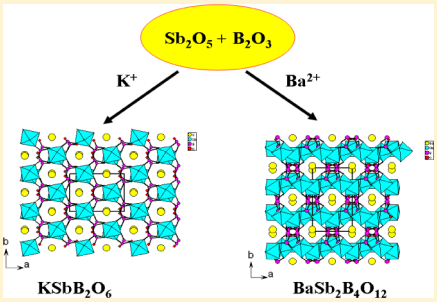

INTRODUCTION

Metal borates have received considerable research attention, mainly due to their rich structural chemistry and important applications as Second-Order Nonlinear Optical (NLO) materials, among which LiB_3O_5 (LBO) and β-BaB_2O_4 (BBO) have been widely used in frequency conversion, optical parameter oscillator (OPO), and signal communication.[1,2] The introduction of BeO_4 tetrahedra into the metal borates afforded a variety of metal beryllium borates with novel layered or 3D anionic frameworks and a number of promising deep Ultraviolet NLO materials, such as $KBe_2BO_3F_2$ (KBBF).[1,3,4] The combination of borates with oxo anions of group 13, 14, and 15 elements led to a variety of new open framework materials such as aluminoborates,[5] galloborate,[6] borosilicates,[7] borogermanates,[8] borophosphates,[9] and boroarsenates.[10] Recently, our group discovered a series of open framework materials that contain both a borate and selenite group with a lone pair, among which NLO-active $Se_2B_2O_7$ features a neutral three-dimensional (3D) framework composed of B_2O_7 corner-sharing with Se(IV)O_3 groups, whereas $K_2Se_3B_2O_{10}$, $ASeB_3O_7$ (A = Na, K), and $Li_2SeB_8O_{15}$ display 1D, 2D, and 3D anionic frameworks, respectively.[11] Unlike metal borophosphates and boroarsenates, little is known about boroantimonates and boroantimonites.[12] The only structurally characterized stoichiometric boroantimonate is $K_3BSb_4O_{13}$, whose structure features a novel three-dimensional network composed of hexagonal bronze-like 2D (Sb_3O_9) layers that are cross-linked alternatively by edge-sharing Sb_2O_{10} dimers and BO_3 triangles, forming 1D interconnected tunnels running along the ***a*** and ***b*** directions, which are filled by K^+ ions. It is believed that many new boroantimonates can be obtained by replacing K^+ with other alkali or alkaline earth metal ions and changing B/Sb molar ratios, as well as other reaction conditions. Hence we started a research program to explore metal boroantimonates systematically. Our such research efforts led to the discovery of two new metal boroantimonates, namely, polar $KSbB_2O_6$ and centrosymmetric $BaSb_2B_4O_{12}$. Herein we report their syntheses, crystal structures, and physical properties.

EXPERIMENTAL SECTION

Materials and Methods. All of the chemicals were analytically pure from commercial sources and used without further purification. K_2CO_3 (≥99.0+%, Shantou Guanghua Chemical Factory), $Ba(OH)_2 \cdot 8H_2O$ (≥98.0+%, Sinopharm Chemical Reagent Co. Ltd.), Sb_2O_3 (≥98.0+%, Zheng'an Chemical Factory), Sb_2O_5 (≥99.998+%, Alfa Aesar), H_3BO_3 (≥99. 8+%, Aladdin Chemistry Co. Ltd.), and B_2O_3 (≥98.0+%, Shanghai Chemical Reagent Company). Microprobe elemental analyses were performed on a field emission scanning electron microscope (FESEM, JSM6700F) equipped with an energy dispersive X-ray spectroscope (EDS, Oxford INCA). X-ray powder diffraction (XRD) patterns were collected on a Panalytical X'pert Pro MPD diffractometer using graphite-monochromated Cu–Kα radiation in the 2θ range of 5–80° with a step size of 0.02°. IR spectra were recorded on a Magna 750 FT-IR spectrometer as KBr pellets in the range of 4000–400 cm^{-1}. Optical diffuse reflectance spectra were measured at room temperature with a PE Lambda 900 UV–vis spectrophotometer. $BaSO_4$ plate was used as a standard (100%

Received: January 24, 2014
Published: March 25, 2014

   dx.doi.org/10.1021/ic5001842 | Inorg. Chem. 2014, 53, 3847–3853

reflectance). The absorption spectrum was calculated from reflectance spectra using the Kubelka–Munk function: $\alpha/S = (1 - R)^2/2R$,[13] where α is the absorption coefficient, S is the scattering coefficient, which is practically wavelength independent when the particle size is larger than 5 μm, and R is the reflectance. Thermogravi-metric analyses were carried out with a NETZSCH STA 449C unit at a heating rate of 10 °C/min under a N_2 atmosphere. The measurements of Second Harmonic Generation (SHG) were carried out on the sieved (70–100 mesh) powder samples of $KSbB_2O_6$ by using the Kurtz and Perry method with a 1064 nm Q-switch laser.[14] The ferroelectric property of $KSbB_2O_6$ was measured on an aixACCT TF Analyzer 2000 ferroelectric tester at room temperature.[15] $KSbB_2O_6$ powder was pressed into a pellet (10-mm-diameter and 0.9-mm-thick) and the conducting Ag-glue was applied on the both sides of the pellet surfaces for electrodes.

Syntheses of $KSbB_2O_6$ and $BaSb_2B_4O_{12}$. Single crystals of the two compounds were obtained by high-temperature solid state reactions of K_2CO_3 (or $Ba(OH)_2{\cdot}8H_2O$), Sb_2O_3, and H_3BO_3. The mixture of K_2CO_3 or $Ba(OH)_2{\cdot}8H_2O$, Sb_2O_3, and H_3BO_3 was ground in an agate mortar and transferred to platinum crucibles. The loaded compositions are as follows: K_2CO_3 (0.60 mmol, 0.0829 g), Sb_2O_3 (0.80 mmol, 0.2332 g), and H_3BO_3 (4 mmol, 0.2474 g) for $KSbB_2O_6$; $Ba(OH)_2{\cdot}8H_2O$ (1 mmol, 0.3155 g), Sb_2O_3 (1 mmol, 0.2915 g), and H_3BO_3 (4 mmol, 0.2474 g) for $BaSb_2B_4O_{12}$. For both compounds, the mixtures were heated at 850 °C for 33 h and then cooled to 300 °C at a rate of 5 °C/h before the furnace was switched off. The average atomic ratios of K/Sb and Ba/Sb determined by Energy-Dispersive Spectrometry (EDS) on several single crystals are 0.97:1 and 0.48:1, respectively, which are in good agreement with those determined from single-crystal X-ray structure analyses. During the reactions, Sb^{3+} has been oxidized to Sb^{5+} by oxygen at high temperature. After proper structural analyses, pure polycrystalline samples of the two compounds were obtained quantitatively by the solid-state reactions of a K_2CO_3 or $Ba(OH)_2{\cdot}8H_2O/Sb_2O_5/B_2O_3$ mixture in a molar ratio of 1:1:2. The initial mixture was ground thoroughly in an agate motor and then heated at 750 °C for $KSbB_2O_6$ or 800 °C for $BaSb_2B_4O_{12}$ for 4 days with several intermediate grindings and then cooled to 300 °C at a rate of 5 °C/h. Their purities were confirmed by power XRD diffraction studies (Supporting Information, SI, Figures S1). IR data (KBr cm^{-1}): 1337 (s), 1220 (s), 1042 (m), 926 (w), 899 (w), 799 (m), 722 (m), 697 (m), 672 (m), 650 (m), 584 (m), 518 (m), 463(w) for $KSbB_2O_6$; and 1346 (s), 1310 (s), 1206 (s), 1038 (m), 888 (w), 816 (s), 714 (m), 662 (m), 640 (m), 564 (m), 534 (w), 505 (w), and 458(m) for $BaSb_2B_4O_{12}$ (SI Figure S2).

Single-Crystal Structure Determination. Data collections for single crystals of $KSbB_2O_6$ and $BaSb_2B_4O_{12}$ with dimensions of 0.2 × 0.08 × 0.04 mm^3 and 0.08 × 0.04 × 0.03 mm^3 were performed on a Rigaku Saturn724 CCD diffractometer equipped with a graphite-monochromated Mo–Kα radiation (λ = 0.71073 Å) at 293(2) K. The data sets were corrected for Lorentz and polarization factors as well as for absorption by the multiscan method.[15a] Both structures were solved by direct methods and refined by a full-matrix least-squares fitting on F^2 by SHELX-97.[15b] Both structures were checked for possible missing symmetry elements by using PLATON.[15c] The Flack factor of 0.03(3) for $KSbB_2O_6$ with a polar space group of Cc confirmed the correctness of its absolute structure. Crystallographic data and structural refinements for both compounds are summarized in Table 1. Important bond distances are listed in Table 2. More details on the crystallographic studies are given in the SI.

Computational Descriptions. Single crystal structural data of the two compounds were used for the theoretical calculations. Band structures and density of states (DOS) were performed with the total-energy code CASTEP.[16] The total energy is calculated with density functional theory (DFT) using Perdew-Burke-Ernzerhof (PBE) generalized gradient approximation.[17] The interactions between the ionic cores and the electrons were described by the norm-conserving pseudopotential.[18] The following orbital electrons were treated as valence electrons: K-$3s^23p^64s^1$, Ba-$5s^25p^66s^2$, Sb-$5s^25p^3$, B-$2s^22p^1$, and O-$2s^22p^4$. The numbers of plane waves included in the basis sets were determined by a cutoff energy of 500 eV for the two compounds, and the numerical integration of the Brillouin zone is performed using a 4 × 4 × 2, 4 × 3 × 3 Monkhorst-Pack k-point sampling for $KSbB_2O_6$

Table 1. Summary of Crystal Data and Structural Refinements for the Two Compounds

compound	$KSbB_2O_6$	$BaSb_2B_4O_{12}$
Fw	278.47	616.08
crystal system	monoclinic	monoclinic
space group	Cc (no. 9)	$C2/c$ (no. 15)
a (Å)	11.458(14)	6.9818(14)
b (Å)	7.019(14)	11.8452(19)
c (Å)	7.324(14)	11.089(3)
β (deg)	124.413(16)	102.772(14)
V (Å^3)	485.9(15)	894.4(3)
Z	4	4
D_{calcd} (g·cm^{-3})	3.806	4.575
μ(Mo–Kα) (mm^{-1})	6.485	10.424
GOF on F^2	1.096	1.094
flack factor	0.03(3)	none
$R1$, w$R2$ ($I > 2\sigma(I)$)	0.0219, 0.0518	0.0210, 0.0498
(observed data) all data) ($I > 2\sigma(I)$)a	0.0246, 0.0521	0.0219, 0.0503

[a] $R1 = \sum||Fo| - |Fc||/\sum|Fo|$, w$R2 = \{\sum w[(Fo)^2 - (Fc)^2]^2/\sum w[(Fo)^2]^2\}^{1/2}$.

Table 2. Important Bond Lengths (Å) and Angles (°) for the Two Compounds[a]

	$KSbB_2O_6$[b]		
K(1)–O(3)#1	2.681(6)	K(1)–O(2)#2	2.815(5)
K(1)–O(1)	2.861(7)	K(1)–O(6)#3	2.881(5)
K(1)–O(4)#4	2.922(5)	K(1)–O(5)#5	2.958(5)
K(1)–O(5)#3	2.970(7)	K(1)–O(3)#2	2.994(6)
K(1)–O(4)	3.027(6)	K(1)–O(2)#1	3.030(6)
Sb(1)–O(1)	1.943(6)	Sb(1)–O(1)#6	1.949(6)
Sb(1)–O(6)#5	1.960(4)	Sb(1)–O(2)#7	1.971(4)
Sb(1)–O(3)	1.977(4)	Sb(1)–O(4)	1.994(4)
B(1)–O(4)	1.344(7)	B(1)–O(6)	1.357(7)
B(1)–O(5)	1.407(7)	B(2)–O(2)	1.343(7)
B(2)–O(3)	1.370(6)	B(2)–O(5)	1.387(7)
	$BaSb_2B_4O_{12}$[c]		
Ba(1)–O(1)#1	2.810(3)	Ba(1)–O(1)#2	2.810(3)
Ba(1)–O(6)#3	2.862(3)	Ba(1)–O(6)#4	2.862(3)
Ba(1)–O(3)#5	2.899(3)	Ba(1)–O(3)	2.899(3)
Ba(1)–O(5)#1	3.053(3)	Ba(1)–O(5)#2	3.053(3)
Ba(1)–O(4)#3	3.180(3)	Ba(1)–O(4)#4	3.180(3)
Ba(1)–O(2)#5	3.258(3)	Ba(1)–O(2)	3.258(3)
Sb(1)–O(1)	1.937(4)	Sb(1)–O(1)#5	1.937(4)
Sb(1)–O(3)#6	1.979(3)	Sb(1)–O(3)#7	1.979(3)
Sb(1)–O(6)#4	1.980(3)	Sb(1)–O(6)#3	1.980(3)
Sb(2)–O(1)	1.952(4)	Sb(2)–O(1)#8	1.952(4)
Sb(2)–O(5)	1.965(3)	Sb(2)–O(5)#8	1.965(3)
Sb(2)–O(2)#8	1.984(3)	Sb(2)–O(2)	1.984(3)
B(1)–O(3)	1.356(6)	B(1)–O(2)	1.374(6)
B(1)–O(4)	1.399(6)	B(2)–O(5)	1.360(6)
B(2)–O(6)	1.374(6)	B(2)–O(4)	1.399(6)

[a] Symmetry transformations used to generate equivalent atoms. [b] For $KSbB_2O_6$: #1 x, y+1, z; #2 x, $-y$, z+1/2; #3 x+1/2, y+1/2, z+1; #4 x, $-y$+1, z+1/2; #5 x+1/2, $-y$+1/2, z+1/2; #6 x, $-y$, z−1/2; #7 x+1/2, $-y$−1/2, z+1/2. [c] For $BaSb_2B_4O_{12}$: #1 x+1/2, y+1/2, z; #2 $-x$+1/2, y+1/2, $-z$+1/2; #3 $-x$, y, $-z$+1/2; #4 x+1, y, z; #5 $-x$+1, y, $-z$+1/2; #6 $-x$+1/2, y−1/2, $-z$+1/2; #7 x+1/2, y−1/2, z; #8 $-x$+1/2, $-y$+1/2, $-z$+1.

dx.doi.org/10.1021/ic5001842 | Inorg. Chem. 2014, 53, 3847–3853

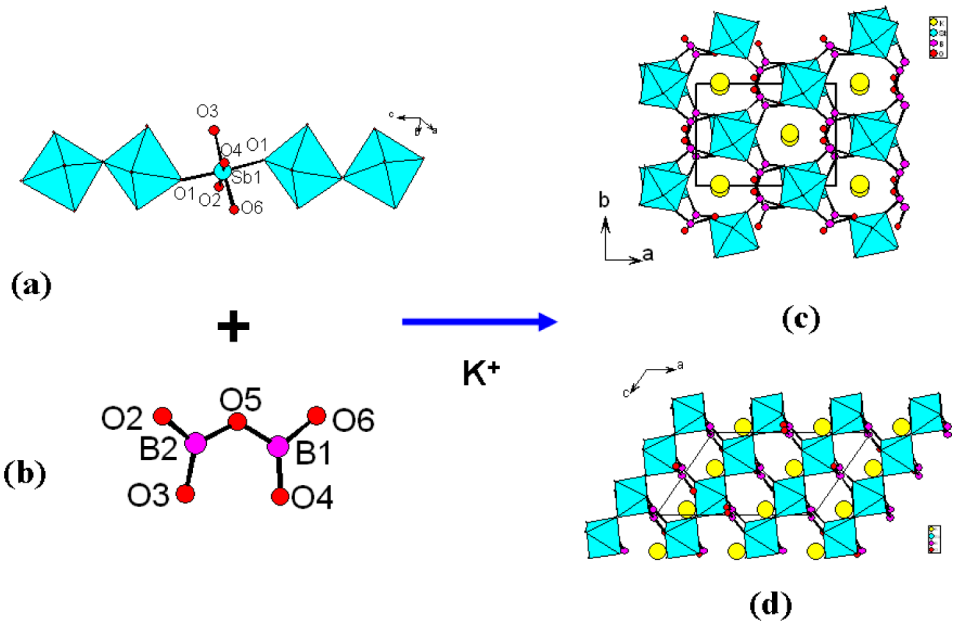

Figure 1. A 1D antimony oxide chain along *c*-axis (a), a B_2O_5 group (b), and view of the structure of $KSbB_2O_6$ along *c* and *b* axes (c and d).

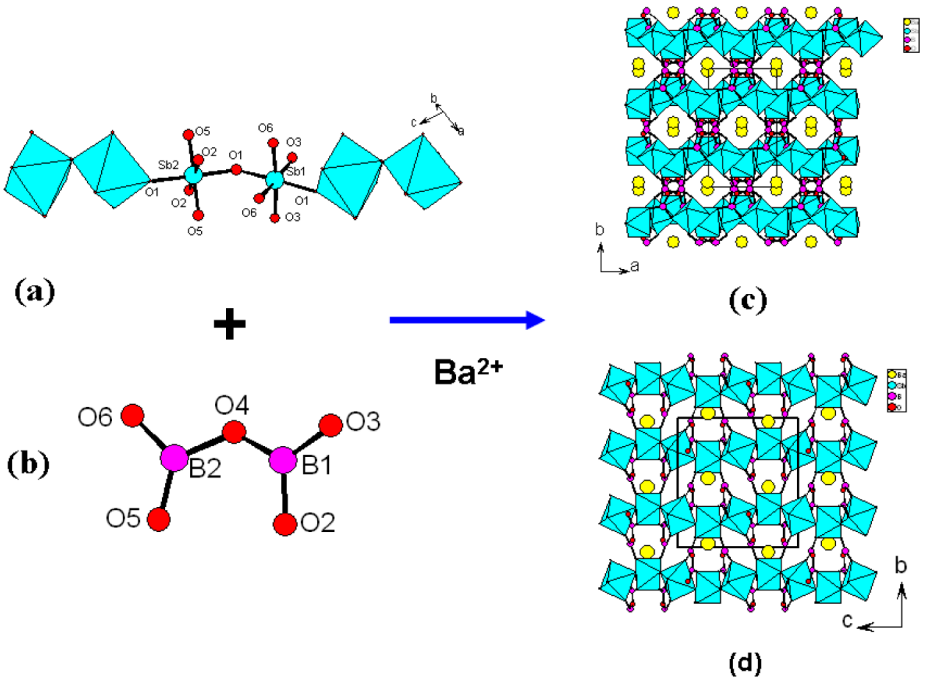

Figure 2. A 1D antimony oxide chain along [101] direction (a), a B_2O_5 group (b), and view of the structure of $KSbB_2O_6$ along *c* and *a* axes (c and d).

and $BaSb_2B_4O_{12}$, respectively. The other parameters and convergent criteria were the default values of the CASTEP code.

RESULTS AND DISCUSSION

Two novel boroantimonates, namely, $KSbB_2O_6$ and $BaSb_2B_4O_{12}$ have been successfully synthesized through high temperature solid-phase reactions. They represent the second and third members of the structurally characterized boroantimonates. Their structures feature two types of 3D anionic frameworks with 1D tunnels along *c*-axis that are filled by K^+ or Ba^{2+} cations.

Crystal Structure of $KSbB_2O_6$. $KSbB_2O_6$ crystallizes in polar space group *Cc*, its structure features a novel 3D anionic boroantimonate network with 1D tunnels of Sb_3B_4 7-membered-rings (MRs) along *c*-axis and 1D tunnels of Sb_4B_2 6-MRs along *b*-axis, both of which are filled by K^+ ions (Figure 1). The 3D framework is based on 1D chains of corner-sharing SbO_6 octahedra which are further bridged by B_2O_5 groups through Sb−O−B bridges (Figure 1). The asymmetric $KSbB_2O_6$ contains one K, one Sb, one B_2O_5 group as well as an oxide anion, all of them at general sites. The Sb atom is octahedrally coordinated by two oxide anions and four oxygen atoms from three B_2O_5 groups (one is in a bidentate chelation

dx.doi.org/10.1021/ic5001842 | Inorg. Chem. 2014, 53, 3847−3853

fashion and the other two in a unidentate fashion) (Figure S3a). The Sb−O distances are in the range of 1.943(6)-1.994(4) Å, and the *cis* and *trans* O−Sb−O bond angles are in the ranges of 81.2(2)−99.4(2) and 169.3(2)−172.96(9)°, respectively. Hence the SbO_6 octahedron is only slightly distorted. These bond distances and angles are close to those reported in $K_3BSb_4O_{13}$.[12] Both B atoms of the B_2O_5 group are 3-coordinated with a planar triangular geometry and B−O distances are in the range of 1.343(7)−1.407(7) Å. These two BO_3 groups share a corner to form a B_2O_5 group, which is different from the "isolated" BO_3 groups in $K_3BSb_4O_{13}$.[12]

Neighboring SbO_6 octahedra are interconnected via corner-sharing into a 1D chain along *c*-axis (Figure 1a). Such 1D chains are bridged by B_2O_5 groups into a novel 3D network with 1D tunnels of Sb_3B_4 7-membered-rings (MRs) along *c*-axis and 1D tunnels of Sb_4B_2 6-MRs along *b*-axis, both of which are filled by K^+ ions (Figure 1c,d). The B−O−Sb bond angles fall in the range of 124.8(4)−137.7(3) °. The K^+ ion is 10-coordinated by 10 oxygen atoms with K−O distances in the range of 2.681(6)−3.030(6) Å. Bond-valence calculations revealed that the K, B, and Sb atoms are in an oxidation state of +1, +3, and +5, respectively, the calculated total bond valences for K(1), B(1), B(2), and Sb(1) atoms are 1.25, 3.02, 3.03, and 5.63, respectively.[19]

It is interesting to compare the structure of $KSbB_2O_6$ with that of $K_3BSb_4O_{13}$,[12] which is an antimony-rich phase, its structure features a novel three-dimensional network composed of hexagonal bronze-like 2D (Sb_3O_9) layers that are cross-linked alternatively by edge-sharing Sb_2O_{10} dimers and BO_3 triangles, forming 1D tunnels of Sb_8 8-MRs and Sb_4B_2 6-MRs along both *a* and *b* axes, which are filled by K^+ ions.

Crystal Structure of $BaSb_2B_4O_{12}$. $BaSb_2B_4O_{12}$ crystallizes in centrosymmetric space group *C*2/*c*, its structure features a different 3D anionic boroantimonate network with 1D tunnels of Sb_4B_4 8-membered-rings (MRs) along *c*-axis and 1D tunnels of Sb_2B_4 6-MRs along *a*-axis, both of which are filled by Ba^{2+} ions (Figure 2). Similar to that of $KSbB_2O_6$, the 3D anionic framework of $BaSb_2B_4O_{12}$ is also based on 1D chains of corner-sharing SbO_6 octahedra which are further bridged by B_2O_5 groups through Sb−O−B bridges (Figure 2). The asymmetric unit of $BaSb_2B_4O_{12}$ contains Ba(1) and Sb(1) at a site of 2-fold rotation axis, Sb(2) at inversion center, a B_2O_5 group as well as an oxide anion at the general sites. The Sb(1) atom is octahedrally coordinated by two oxide anion and four oxygen atoms from four B_2O_5 groups in a unidentate fashion whereas the Sb(2) atom is octahedrally coordinated by two oxide anions and four oxygen atoms from two B_2O_5 groups in a bidentate chelating fashion (SI Figure S3b). The Sb−O distances are in the range of 1.937(4)−1.984(3) Å. Hence both SbO_6 octahedra are also slightly distorted. These bond distances are close to those in $KSbB_2O_6$ and $K_3BSb_4O_{13}$.[12] Both B atoms of the B_2O_5 group are 3-coordinated with a planar triangular geometry and B−O distances are in the range of 1.356(6)−1.399(6) Å.

Neighboring SbO_6 octahedra are interconnected via corner-sharing into a 1D antimony oxide chain along the [101] direction (Figure 2a). Such 1D chains are bridged by B_2O_5 groups into a novel 3D network with 1D tunnels of Sb_4B_4 8-membered-rings (MRs) along *c*-axis and 1D tunnels of Sb_2B_4 6-MRs along *a*-axis, both of which are filled by Ba^{2+} ions (Figure 2c,d). The B−O−Sb bond angles fall in the range of 123.6(3)−131.5(3)°. The Ba^{2+} ion is 12-coordinated by 12 oxygen atoms with Ba−O distances in the range of 2.810(3)−3.258(3) Å. Bond-valence calculations suggest that the Ba, B, and Sb atoms are in an oxidation state of +2, +3, and +5, respectively, the calculated total bond valences for Ba(1), B(1), B(2), Sb(1), and Sb(2) atoms are 1.88, 2.96, 2.95, 5.64, and 5.61, respectively.[19]

Although the 3D frameworks of $KSbB_2O_6$ and $BaSb_2B_4O_{12}$ are both based on 1D chains of corner-sharing SbO_6 octahedra and B_2O_5 groups, their networks display several differences. First, the 1D chains of corner-sharing SbO_6 octahedra are extended in different directions, along the *c*-axis in the K phase whereas in the [101] direction in the Ba phase. Second, the coordination geometries around the Sb atoms are also slightly different, as discussed. Third, the 1D tunnels of the networks in above two compounds display different ring systems, the K phase exhibits 1D tunnels of the anionic frameworks of 7- and 6- MRs along *b*- and *c*-axes, respectively, whereas the Ba phase shows the 1D tunnels of 6- and 8-MRs along *a*- and *c*-axes, respectively. These differences are caused mainly by the different charges and ionic radii of K^+ and Ba^{2+} ions. The $[Sb_2B_4O_{12}]^{2-}$ in $BaSb_2B_4O_{12}$ is doubled compared with the $[SbB_2O_6]^-$ in $KSbB_2O_6$, hence the cell volume of the Ba compound is also almost doubled compared with that of the K compound.

It is also interesting to study the topological structures for the above two compounds. For both compounds, the B_2O_5 group forms a bidentate chelation with a Sb atom and also bridges with two other Sb atoms, hence it is a three connected node. The SbO_6 octahedron in $KSbB_2O_6$ is connected to two other SbO_6 octahedra and three B_2O_5 groups, hence it is a five-connected node. Hence the topology of $KSbB_2O_6$ is a hms type 3D 3,5-nodal net with Schläfli symbol of $\{6^3\}\{6^9.8\}$ (Figure 3a).[20] The two unique Sb atoms in $BaSb_2B_4O_{12}$ show different coordination environment, the $Sb(1)O_6$ unit is corner-sharing with two other SbO_6 units and four B_2O_5 groups, whereas the $Sb(2)O_6$ unit is connected to two other SbO_6 units and two B_2O_5 groups, hence Sb(1) and Sb(2) atoms are 6 and 4-connected nodes, respectively. From a topological viewpoint, the anionic network of $[Sb_2B_4O_{12}]^{2-}$ in $BaSb_2B_4O_{12}$ can also be described as a new 3, 4, 6-trinodal topological type with the Schläfli symbol of $\{5^2.6^2.7.8\}\{5^2.6\}_2\{5^3.6^4.7^5.8^3\}$ (Figure 3b).

It is interesting to note that the different size and charge of the cation have strong effects on the overall centricity of the network formed. For $KSbB_2O_6$, when viewed from *b* axis, there are uniform 1D tunnels of Sb_4B_2 rings which are filled by K^+ ions (Figure 1d), and the B_2O_5 groups are alligned to produce a net macroscopic polarization along the [−101] direction, hence $KSbB_2O_6$ is a polar material. In $BaSb_2B_4O_{12}$, when viewed from the *a* axis, two types of 1D tunnels based on Sb_4B_2 and Sb_2B_4 rings, respectively, are formed. Due to the higher cationic charges of Ba^{2+}, only larger 1D tunnels based on Sb_2B_4 rings are filled by Ba^{2+} cations, whereas the smaller ones based on Sb_4B_2 rings are vacant (Figure 2d). Also, the neighboring B_2O_5 groups are oriented toward different directions, hence $BaSb_2B_4O_{12}$ is censtrosymmetric (CS). Similar cationic effects on the overall centricities of the structures formed have been previously reported.[21]

Thermal Stability Studies. TGA studies indicate that both $KSbB_2O_6$ and $BaSb_2B_4O_{12}$ are all thermally stable up to about 1000 °C. Then they began to lose weight at about 1100 °C (Figure 4).

Optical Properties. IR spectra of $KSbB_2O_6$ and $BaSb_2B_4O_{12}$ indicate that they are transparent in the range of 4000−1500 cm^{-1} (2.5−6.7 μm) (SI Figure S2). The antisymmetric stretching vibrations of BO_3 are shown in 1038−1346 cm^{-1}. The symmetric stretching vibrations of BO_3 are shown in 714−

dx.doi.org/10.1021/ic5001842 | *Inorg. Chem.* 2014, 53, 3847−3853

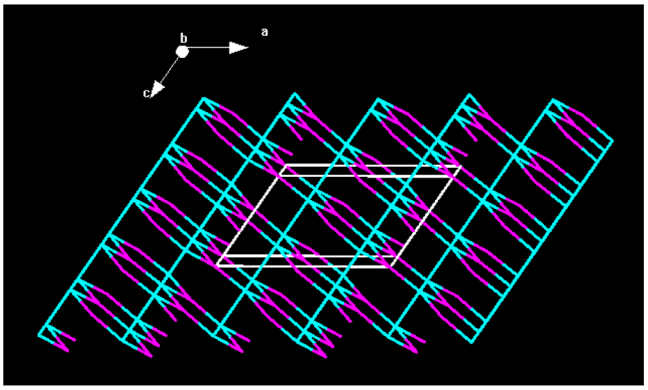

(a)

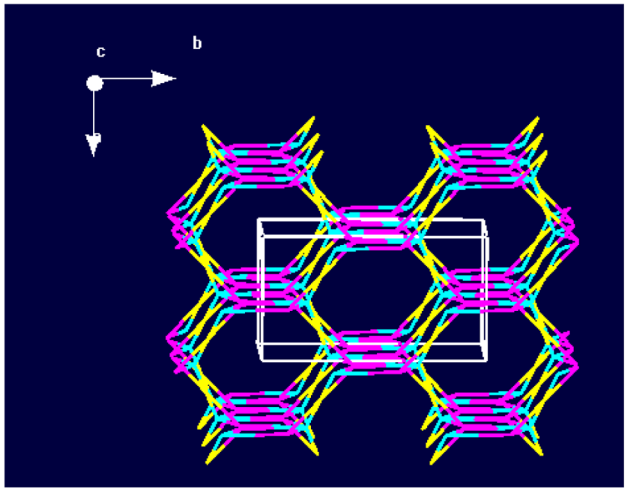

(b)

Figure 3. The topological view of the hms type 3D 3,5-nodal net with Schläfli symbol of $\{6^3\}\{6^9.8\}$ for the anionic structure in $KSbB_2O_6$, the pink and cyan balls represent the three- and five-connected node, respectively (a); and a new 3, 4, 6-trinodal topological type with the Schläfli symbol of $\{5^2.6^2.7.8\}\{5^2.6\}_2\{5^3.6^4.7^5.8^3\}$ for the anionic structure in $BaSb_2B_4O_{12}$, the pink, yellow, and cyan balls represent the three-, four-, and six-connected node, respectively (b).

926 cm^{-1}. The bending vibrations of BO_3 are also shown in 458−697 cm^{-1}. These assignments are inconsistent with those previously reported.[2−4]

UV absorption spectra of $KSbB_2O_6$ and $BaSb_2B_4O_{12}$ show little absorption in the range of 500−2500 nm (0.5−2.5 μm) (SI Figure S4). Optical diffuse reflectance spectrum studies indicate that $KSbB_2O_6$ and $BaSb_2B_4O_{12}$ are semiconductors with optical band gaps of 3.63 and 4.26 eV, respectively (SI Figure S5).

Second Harmonic Generation (SHG) Properties. Since $KSbB_2O_6$ crystallized in a noncentrosymmetric and polar space group, it is worthy to study its second-harmonic generation (SHG) properties. SHG measurements on a 1064 nm Q-switch laser revealed that $KSbB_2O_6$ exhibits a very weak SHG response. On the basis of structural data, the distortion of SbO_6 octahedron is very small. The calculated dipole moments for the SbO_6 and B_2O_5 units are 1.70 and 2.45 D, respectively, and the net dipole moment for a unit cell is 6.06 D (Table 3), which is very small compared with other polar materials with large SHG responses, such as 129.48 D for $K(VO)_2O_2(IO_3)_3$ with an SHG response of 3.6 × $KTiOPO_4$ (KTP) and 230.85 D for $PbPt(IO_3)_6(H_2O)$ with a SHG response of about 8 × KDP

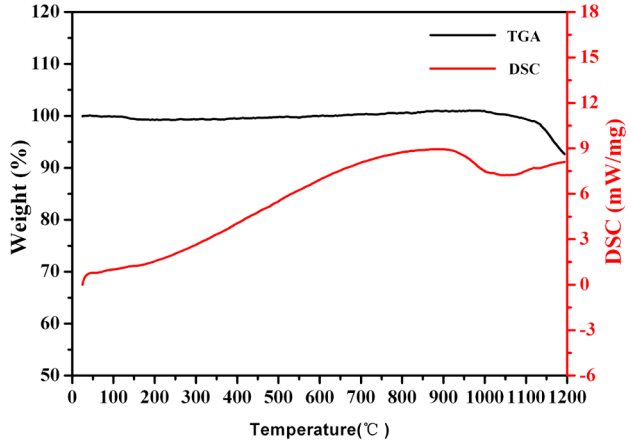

(a)

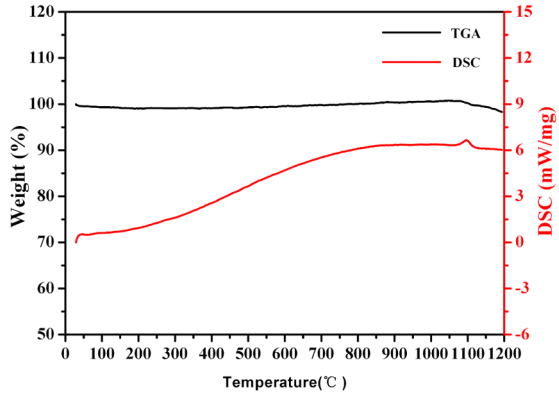

(b)

Figure 4. TGA and DTA curves for $KSbB_2O_6$ (a) and $BaSb_2B_4O_{12}$ (b).

Table 3. Calculation of Dipole Moments for the B_2O_5 Groups, SbO_6 Octahedra and the Net Dipole Moment for a Unit Cell in $KSbB_2O_6$ (D = Debye)

polar unit	polar unit number in a unit cell	dipole moment (μ, unit: Debye)			
		x-component	*y*-component	*z*-component	total magnitude
B_2O_5	4	−0.71	±1.72	−1.58	2.45
SbO_6	4	−0.29	±1.62	0.44	1.70
net dipole moment in a unit cell		−4.00	0	−4.56	6.06

(KH_2PO_4).[22] Hence, the dipole moments asociated with SbO_6 octahedra and B_2O_5 groups in $KSbB_2O_6$ have largely been canceled out, which resulted in only a weak SHG response.

Polarization Measurement. The polarization measurement of $KSbB_2O_6$ was investigated because it crystallized in polar point group (*Cc*) required for the possible of ferroelectric behavior. Polarization measurement on a pellet (10-mm-diameter and 0.9-mm-thick) for $KSbB_2O_6$ revealed a very small remanent polarization (Pr) of 0.055 $\mu C/cm^2$ (SI Figure S6), hence the ferroelectric property is negligible. On the basis of SHG measurements, the net polarization from SbO_6 octahedra and B_2O_5 groups is very small. Hence the polarization reversibility may be limited to the very small contribution from slightly distorted SbO_6 octahedra and B_2O_5 groups or from dielectric loss.

Theoretical Studies. To gain further insights on the electronic structure and optical properties of $KSbB_2O_6$ and $BaSb_2B_4O_{12}$, theoretical calculations based on DFT methods

dx.doi.org/10.1021/ic5001842 | Inorg. Chem. 2014, 53, 3847−3853

were made. The calculated band structures of $KSbB_2O_6$ and $BaSb_2B_4O_{12}$ along high symmetry points of the first Brillouin zone are plotted in SI Figure S7. The state energies (eV) of the lowest conduction band (L-CB) and the highest valence band (H-VB) of the two compounds are listed in SI Table S1. The calculated band structures (SI Figure S7 and Table S1) indicate that both compounds are direct band gap semiconductors with band gaps of 3.61 and 3.94 eV for $KSbB_2O_6$ and $BaSb_2B_4O_{12}$, respectively. The calculated band gaps are close to the experimental values (3.63 eV for $KSbB_2O_6$, and 4.26 eV for $BaSb_2B_4O_{12}$).

The bands can be assigned according to the total and partial densities of states (DOS) as plotted in Figure 5. It is clear that

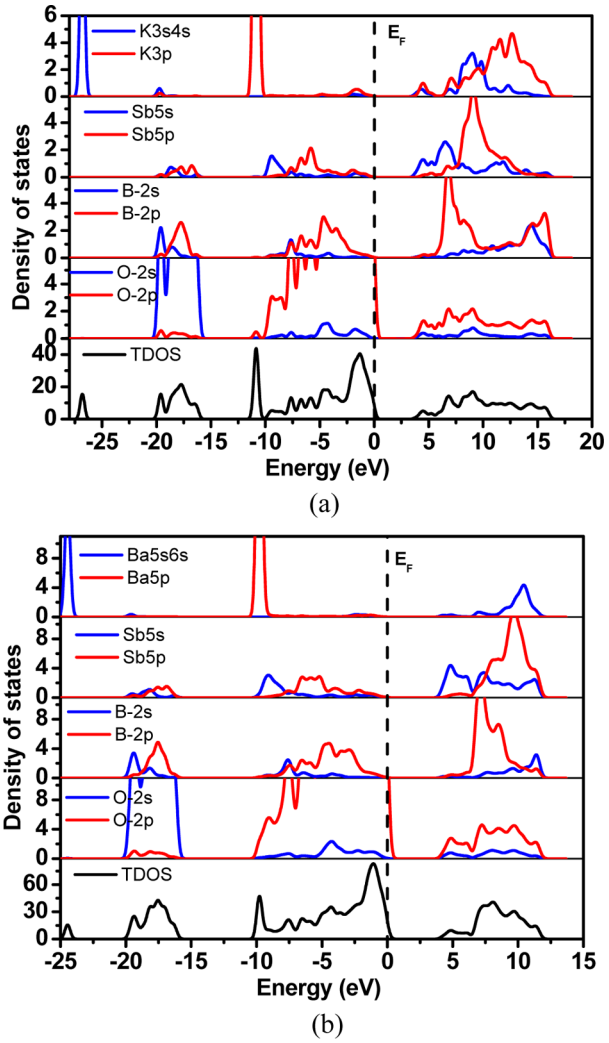

Figure 5. The total density of states and partial density of states of $KSbB_2O_6$ (a) and $BaSb_2B_4O_{12}$ (b) (the Fermi level is set at 0 eV).

the DOSs of two compounds behave very similar to each other, so we take $KSbB_2O_6$ as an example to describe them in details. For $KSbB_2O_6$ (Figure 5a), the bottom-most valence bands ranging from −28 to −25 eV originate from K-3s states. The bands between −20 and −15 eV are composed of O-2s, B-2s2p, and Sb-5s5p states, and the peak localized at −11.0 eV arises from K-3p states. We will focus on the VB and the CB in the vicinity of the Fermi level (between −10.0 and 17 eV), which counts for most of the bonding character in a compound. It is obvious that in that region, Sb-5s5p and B-2s2p states overlap fully with O-2p states, indicative of the well-defined Sb−O and B−O covalent interactions.

CONCLUSIONS

In summary, two new boroantimonates, namely, $KSbB_2O_6$ and $BaSb_2B_4O_{12}$, have been successfully synthesized through high-temperature solid state reactions. Their structures feature two types of novel 3D anionic frameworks composed of 1D chains of corner-sharing SbO_6 octahedra that are interconnected by B_2O_5 groups. It is found that the Sb/B ratio played an important role in the anionic framework formed. $K_3BSb_4O_{13}$ with a B/Sb ratio of 1/4 features a novel three-dimensional network composed of hexagonal bronze-like 2D (Sb_3O_9) layers that are cross-linked alternatively by edge-sharing Sb_2O_{10} dimers and BO_3 triangles, whereas the Sb−O units in $KSbB_2O_6$ and $BaSb_2B_4O_{12}$ with a B/Sb ratio of 2:1 are one-dimensional, and the BO_3 groups are dimerized. It is also anticipated that the combination of borate groups and the lone pair containing SbO_3^{3-} group can lead to a number of polar or noncentrosymmetric boroantimonites with good SHG properties. Our future research efforts will be devoted to the systematic explorations of metal boroantimonates and boroantimonites of alkali and alkaline earth, transition metal, and lanthanide ions.

ASSOCIATED CONTENT

Supporting Information

X-ray crystallographic files in CIF format, simulated and experimental powder XRD patterns, coordination geometries around the Sb atoms, IR, UV-absorption, and optical diffuse reflectance spectra for the two compounds, and the plot of polarization versus applied electric field at different frequencies for $KSbB_2O_6$. This material is available free of charge via the Internet at http://pubs.acs.org.

AUTHOR INFORMATION

Corresponding Author

*Fax: (+86)591-83714946; E-mail: mjg@fjirsm.ac.cn.

Notes

The authors declare no competing financial interest.

ACKNOWLEDGMENTS

This work was supported by the National Natural Science Foundation of China (Grant Nos. 21231006, 21373222, 21203197, and 21001107).

REFERENCES

(1) (a) Becker, P. *Adv. Mater.* **1998**, *10*, 979−992. (b) Chen, C. T.; Wang, Y. B.; Wu, B. C.; Wu, K. C.; Zeng, W. L.; Yu, L. H. *Nature* **1995**, *373*, 322−324. (c) Chen, C. T.; Wu, B. C.; Jiang, A. D.; You, G. M. *Sci. Sin., Ser B* **1984**, *14*, 598−604.

(2) (a) Hagerman, M. E.; Poeppelmeier, K. R. *Chem. Mater.* **1995**, *7*, 602−621. (b) Wu, H. P.; Pan, S. L.; Poeppelmeier, K. R.; Li, H. Y.; Jia, D. Z.; Chen, Z. H.; Fan, X. Y.; Yang, Y.; Rondinelli, J. M.; Luo, H. S. *J. Am. Chem. Soc.* **2011**, *133*, 7786−7790. (c) Wu, H. P.; Yu, H. W.; Yang, Z. H.; Hou, X. L.; Su, X.; Pan, S. L.; Poeppelmeier, K. R.; Rondinelli, J. M. *J. Am. Chem. Soc.* **2013**, *135*, 4215−4218.

(3) (a) Wang, S. C.; Ye, N.; Li, W.; Zhao, D. *J. Am. Chem. Soc.* **2010**, *132*, 8779−8786. (b) Wang, S. C.; Ye, N. *J. Am. Chem. Soc.* **2011**, *133*, 11458−11461.

(4) (a) Huang, H. W.; Yao, J. Y.; Lin, Z. S.; Wang, X. Y.; He, R.; Yao, W. J.; Zhai, N. X.; Chen, C. T. *Angew. Chem., Int. Ed.* **2011**, *50*, 9141−9144. (b) Huang, H. W.; Yao, J. Y.; Lin, Z. S.; Wang, X. Y.; He, R.; Yao, W. J.; Zhai, N. X.; Chen, C. T. *Chem. Mater.* **2011**, *23*, 5457−

5463. (c) Huang, H. W.; Liu, L. J.; Jin, S. F.; Yao, W. J.; Zhang, Y. H.; Chen, C. T. *J. Am. Chem. Soc.* **2013**, *135*, 18319−18322. (d) Yan, X.; Luo, S. Y.; Lin, Z. S.; Yue, Y. C.; Wang, X. Y.; Liu, L. J.; Chen, C. T. *J. Mater. Chem. C* **2013**, *1*, 3616−3622.

(5) (a) Ju, J.; Lin, J. H.; Li, G. B.; Yang, T.; Li, H. M.; Liao, F. H.; Loong, C. K.; You, L. P. *Angew. Chem., Int. Ed.* **2003**, *42*, 5607−5610. (b) Ju, J.; Yang, T.; Li, G. B.; Liao, F. H.; Wang, Y. X.; You, L. P.; Lin, J. H. *Chem.—Eur. J.* **2004**, *10*, 3901−3906. (c) Yang, T.; Bartoszewicz, A.; Ju, J.; Sun, J. L.; Liu, Z.; Zou, X. D.; Wang, Y. X.; Li, G. B.; Liao, F. H.; Martin-Matute, B.; Lin, J. H. *Angew. Chem., Int. Ed.* **2011**, *50*, 12555−12558. (d) Zhou, J.; Fang, W. H.; Rong, C.; Yang, G. Y. *Chem.—Eur. J.* **2010**, *16*, 4852−4863.

(6) (a) Li, R.-K.; Yu, Y. *Inorg. Chem.* **2006**, *45*, 6840−6843. (b) Barbier, J.; Penin, N.; Cranswick, L. M. *Chem. Mater.* **2005**, *17*, 3130−3136. (c) Hu, T.; Hu, C. L.; Kong, F.; Mao, J. G.; Mak, T. C. W. *Inorg. Chem.* **2012**, *51*, 8810−8817. (d) Liu, Z. H.; Yang, P.; Li, P. *Inorg. Chem.* **2007**, *46*, 2965−2967. (e) Cheng, L.; Wei, Q.; Wu, H. Q.; Zhou, L. J.; Yang, G. Y. *Chem.—Eur. J.* **2013**, *19*, 17662−17667.

(7) (a) Wu, H. P.; Yu, H. W.; Pan, S. L.; Huang, Z. J.; Yang, Z. H.; Su, X.; Poeppelmeier, K. R. *Angew. Chem., Int. Ed.* **2013**, *52*, 3406−3410. (b) Parise, J. B.; Gier, T. E. *Chem. Mater.* **1992**, *4*, 1065−1067. (c) Bubnova, R. S.; Stepanov, N. K.; Levin, A. A.; Filatov, S. K.; Paufler, P.; Meyer, D. C. *Solid State Sci.* **2004**, *6*, 629−637.

(8) (a) Dadachov, M. S.; Sun, K.; Conradsson, T.; Zou, X. D. *Angew. Chem., Int. Ed.* **2000**, *39*, 3674−3676. (b) Li, Y. F.; Zou, X. D. *Angew. Chem., Int. Ed.* **2005**, *44*, 2012−2015. (c) Zhang, J. H.; Kong, F.; Xu, X.; Mao, J. G. *J. Solid State Chem.* **2012**, *195*, 63−72 and references therein. (d) X, Xu.; Hu, C. L.; Kong, F.; Zhang, J. H.; Mao, J. G.; Sun, J. L. *Inorg. Chem.* **2013**, *52*, 5831−5837. (e) Hao, Y. C.; Hu, C. L.; Xu, X.; Kong, F.; Mao, J. G. *Inorg. Chem.* **2013**, *52*, 13644−13650.

(9) (a) Kniep, R.; Gozel, G.; Eisenmann, B.; Rohr, C.; Asbrand, M.; Kizilyalli, M. *Angew. Chem., Int. Ed.* **1994**, *33*, 749−751. (b) Moran, K. L.; Gier, T. E.; Harrison, W. T. A.; Stucky, G. D.; Eckert, H.; Elechele, K.; Wasylishen, R. E. *J. Am. Chem. Soc.* **1993**, *135*, 10553−10558.

(10) Wiggin, S. B.; Weller, M. T. *J. Am. Chem. Soc.* **2005**, *127*, 17172−17173.

(11) (a) Kong, F.; Huang, S. P.; Sun, Z. M.; Mao, J. G.; Cheng, W. D. *J. Am. Chem. Soc.* **2006**, *128*, 7750−7751. (b) Zhang, J. H.; Kong, F.; Yang, B. P.; Mao, J. G. *CrystEngCommun.* **2012**, *14*, 8727−8733.

(12) Ftini, M. M.; Haddad, A.; Jouini, T. J. *Chem. Crystallogr* **2000**, *30*, 49−53.

(13) Wendlandt, W. M.; Hecht, H. G. *Reflectance Spectroscopy*; Interscience: New York, 1966.

(14) Kurtz, S. W.; Perry, T. T. *J. Appl. Phys.* **1968**, *39*, 3798−3817.

(15) (a) *CrystalClear*, version 1.3.5; Rigaku Corp.: Woodlands, TX, 1999. (b) Sheldrick, G. M. *SHELXTL, Crystallographic Software Package*, version 5.1; Bruker-AXS: Madison, WI, 1998. (c) Spek, A. L. *PLATON*; Utrecht University: Utrecht, The Netherlands, 2001.

(16) (a) Segall, M. D.; Lindan, P. J. D.; Probert, M. J.; Pickard, C. J.; Hasnip, P. J.; Clark, S. J.; Payne, M. C. *J. Phys.: Condens. Matter* **2002**, *14*, 2717−2744. (b) Milman, V.; Winkler, B.; White, J. A.; Pickard, C. J.; Payne, M. C.; Akhmatskaya, E. V.; Nobes, R. H. *Int. J. Quantum Chem.* **2000**, *77*, 895−910.

(17) Perdew, J. P.; Burke, K.; Ernzerhof, M. *Phys. Rev. Lett.* **1996**, *77*, 3865−3868.

(18) Lin, J. S.; Qteish, A.; Payne, M. C.; Heine, V. *Phys. Rev. B* **1993**, *47*, 4174−4180.

(19) (a) Brown, I. D.; Altermatt, D. *Acta Crystallogr.* **1985**, *B41*, 244−247. (b) Brese, N. E.; O'Keeffe, M. *Acta Crystallogr.* **1991**, *B47*, 192−197.

(20) (a) Lin, J. H.; You, L. P.; Lu, G. X.; Yang, L. Q.; Su, M. Z. *J. Mater. Chem.* **1998**, *8*, 1051−1054. (b) Zhao, W. W.; Pan, S. L.; Han, J.; Zhou, Z. X.; Tian, X. L.; Li, J. J. *Inorg. Chem. Commun.* **2011**, *14*, 566−568.

(21) (a) Lee, D. W.; Ok, K. M.; Chang, H.-Y. *Inorg. Chem.* **2013**, *52*, 5176−5184. (b) Kim, S.-H.; Ok, K. M.; Halasyamani, P. S. *J. Am. Chem. Soc.* **2009**, *131*, 6865−6873.

(22) (a) Sun, C. F.; Hu, C. L.; Xu, X.; Yang, B. P.; Mao, J. G. *J. Am. Chem. Soc.* **2011**, *133*, 5561−5572. (b) Sun, C. F.; Hu, C. L.; Mao, J. G. *Chem. Commun.* **2012**, *48*, 4220−4222.